Supplementary Information Appendix
to
Confinement transition of $\mathbb{Z}_2$ gauge theories coupled to massless fermions: emergent $\mathbf{QCD}_3$ and $SO(5)$ symmetry

Snir Gazit,[1] Fakher F. Assaad,[2] Subir Sachdev,[3,4] Ashvin Vishwanath,[3] and Chong Wang[3]

[1]*Department of Physics, University of California, Berkeley, CA 94720, USA*

[2]*Institut für Theoretische Physik und Astrophysik, Universität Würzburg, 97074 Würzburg, Germany*

[3]*Department of Physics, Harvard University, Cambridge MA 02138, USA*

[4]*Perimeter Institute for Theoretical Physics, Waterloo, Ontario, Canada N2L 2Y5*

Appendix A: Circumventing the zero mode problem at finite Hubbard interactions

To enforce Gauss's law in the numerical simulation [1], we introduce a set of discrete Lagrange multipliers, λ_r, at each lattice site, r, which are identified with the temporal component of the Ising gauge field. Explicitly, for an even LGT $G_r = 1$, we project to the physical Hilbert space using the projector $\hat{P} = \prod_r \hat{P}_r$, where,

$$\begin{aligned}\hat{P}_r &= \frac{1}{2}\left(1 + \prod_{b\in+_r} \sigma^x_{r,b}(-1)^{n^f_r}\right) \\ &= \sum_{\lambda_r=\pm1} e^{i\pi\left(\frac{1-\lambda_r}{2}\right)\left(\sum_{b\in+_r}\left(\frac{1-\sigma^x_{r,b}}{2}\right)+n^f_r\right)}.\end{aligned} \tag{A1}$$

Substituting the above expression in the path integral representation yields the following fermionic weight (see [1] for a complete derivation),

$$W_f(\lambda,\sigma^z) = \mathrm{Tr}\left[e^{i\pi\sum_r\left(\frac{1-\lambda_r}{2}\right)n^f_r}\prod_\tau e^{f^\dagger K(\sigma^z(\tau))f}\right]. \tag{A2}$$

In the above, $K(\sigma^z(\tau))$ is the infinitesimal $\sigma^z(\tau)$-dependent hopping kernel. Remarkably, the constraint does not introduce a sign problem for an arbitrary fermion density. However, at half-filling, configurations satisfying $\prod_r \lambda_r = -1$ sustain an exact zero mode, as can be verified by applying a partial PH symmetry to Eq. (A2). Such configurations have a vanishing Boltzmann weight and are not sampled in the Monte Carlo simulation.

This introduces a systematic bias in expectation values of observables that are not symmetric under partial PH transformation. In Ref. [1], a method that compensates on the missing weight was presented.

In the present work, we consider a simpler solution, explained below. The Hubbard term is decoupled using an auxiliary-field s_r. For attractive interactions the density channel decoupling is given by,

$$e^{\epsilon U\left(n^\uparrow_r-\frac{1}{2}\right)\left(n^\downarrow_r-\frac{1}{2}\right)} = \frac{1}{2}\sum_{s=\pm1} e^{\gamma s_r(n^\downarrow_r+n^\uparrow_r-1)} \tag{A3}$$

where $\gamma = \cosh^{-1}\left(\exp(\epsilon U/2)\right)$. It is clear from the above equation that the associated weight is not symmetric under partial PH transformation for a *generic* auxiliary-field configuration. Therefore for finite Hubbard interactions, the zero mode is lifted allowing for an accurate sampling. We have verified this fact explicitly by benchmarking the QMC data with exact diagonalization on small system sizes.

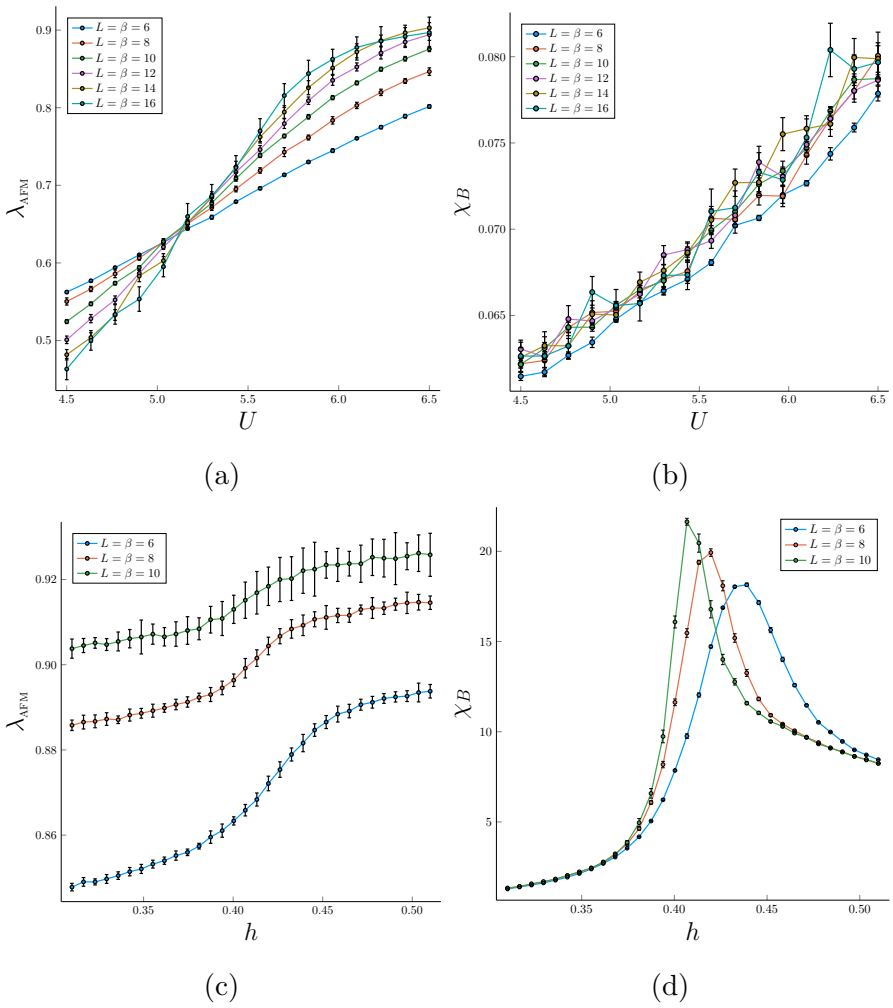

Suppl. Fig. S1: (a-b) AFM ordering transition separating the AFM* and OFM phases. QMC data is calculated at $h = 0.1$ and as a function of U. (a) λ_{AFM} exhibits a clear curve crossing (b) χ_B crosses the transition smoothly. (c-d) Ising confinement transition separating the AFM* and AFM phases. QMC data is calculated at $U = 7$ and as a function of h. (c) λ_{AFM}, indicates that the AFM order remains finite across the transition. (d) The Ising flux susceptibility, χ_B, diverges at the confinement transition with increase in the system size.

Appendix B: Additional QMC data

In this section, we present additional QMC data supporting our finding in the main text. In Fig. S1, we consider two parameter cuts corresponding to the AFM ordering transition between the OSM and AFM* phases and the Ising confinement transition between the AFM* and AFM phases. As expected, we find that the former involves only AFM ordering as seen in a curve crossing analysis of λ_{AFM}, while the latter in marked solely by a singularity in flux susceptibility,

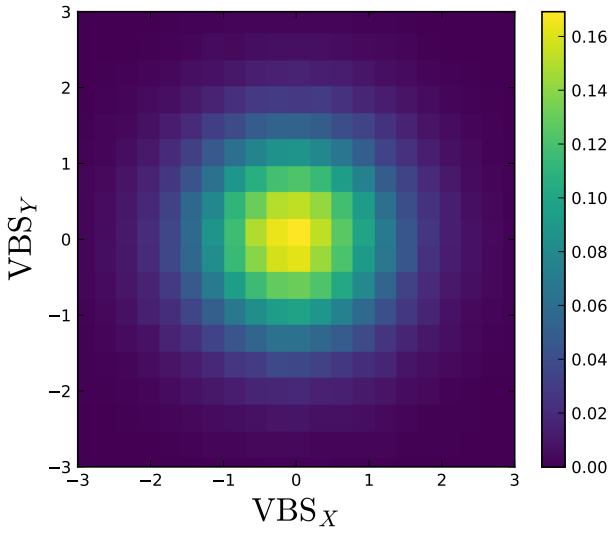

Suppl. Fig. S2: Joint probability distribution $\mathbf{P}(\mathbf{B}^x, \mathbf{B}^y)$ at the OSM confinement transition. The apparent circular symmetry indicates that the C_4 square lattice symmetry is enlarged to an $SO(2)$ rotational symmetry.

χ_B, indicating confinement.

Finally, in Fig. S2, we depict the joint probability distribution, $\mathbf{P}(\mathbf{B}^x, \mathbf{B}^y)$, of the VBS order parameter along the x and y directions, evaluated at the OSM confinement transition. The visible circular symmetry supports the emergence of rotational $SO(2)$ symmetry at the OSM confinement transition.

Appendix C: Dynamically imposed constraint

Imposing the constraint $Q_r = \pm 1$ is necessary to satisfy local $\mathbb{Z}_2$ gauge symmetry. In fact, without a constraint the model is very asymmetric in space and time: $\langle f^\dagger_{r,\alpha}(\tau) f_{r',\alpha'}(\tau = 0)\rangle = \delta_{r,r'}\delta_{\alpha,\alpha'}$. Since G_r commutes with the Hamiltonian, the constraint will be dynamically imposed in the low temperature limit and for observables satisfying $[O, G_r] = 0$, we expect:

$$\lim_{L\to\infty}\lim_{T\to 0}\langle O(\tau)O\rangle_{NC} = \lim_{L\to\infty}\lim_{T\to 0}\langle O(\tau)O\rangle_{C}. \tag{C1}$$

Thus, provided that we first take the zero temperature limit on a finite sized lattice, simulations with, $\langle\bullet\rangle_C$, or without, $\langle\bullet\rangle_{NC}$, constraint should converge to the same result. It is very hard to realize this ordering of limits numerically: as $h \to 0$ the relevant energy scale below which the constraint is dynamically imposed vanishes. Above this energy scale, the Ising fields freeze. The model without constraint is amenable to sign free QMC simulations at odd flavors and may be easier

to simulate with alternative methods such as the fermion bag approach [2]. It is hence certainly worth while comparing results with and without constraint. In this appendix, we briefly present QMC data where the constraint is not explicitly taken into account, and show that consistent results are obtained. We have used the ALF implementation of the auxiliary field QMC algorithm [3]. In contrast to data presented in Ref. [4], we have used parallel tempering schemes as well as global updates to flip blocks of spins along the imaginary time. These approaches aim at reducing the long autocorrelation times we encounter in the vicinity of the OSM to AFM transtion. Fig. **S3** shows the phase diagram at $J/t = -1$ in the U-h plane. We fix the temperature to $\beta t = 80$ such that, as mentioned above, and in the low-h limit the Ising fields freeze and we recover results of the π-flux Hubbard model [5].

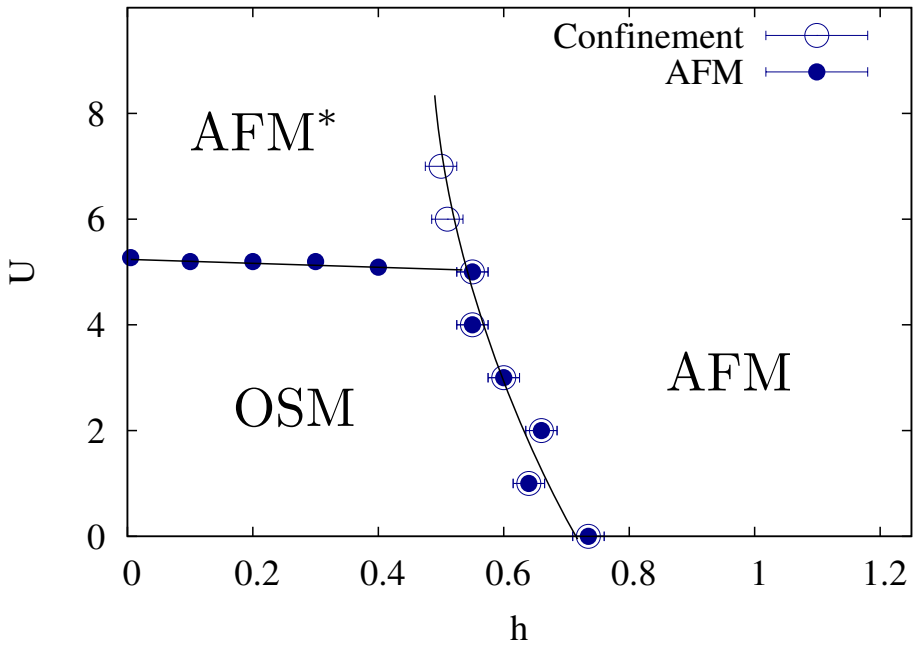

Suppl. Fig. S3: Phase diagram at $J/t = -1$. Data stems from simulations at $L = 10$ and $L = 14$. The AFM transition is obtained by analyzing the renormalization group invariant quantity λ_{AFM}. The confinement transition is obtained by monitoring $\chi_B = \partial\langle\Phi\rangle/\partial h$. We have equally checked that at the confinement transition, visons proliferate. We have used values of $\Delta\tau = 0.4, 0.2, 0.1$ for growing values of U/t.

Figs. **S4** and **S5** plot the VBS and AFM correlation ratios, λ_{AFM} and λ_{VBS} as obtained from the susceptibilities. Both λ_{AFM} and λ_{VBS} are renormalization group invariant quantities and are expected to cross at the critical point. This relies on the assumption that the susceptibility is

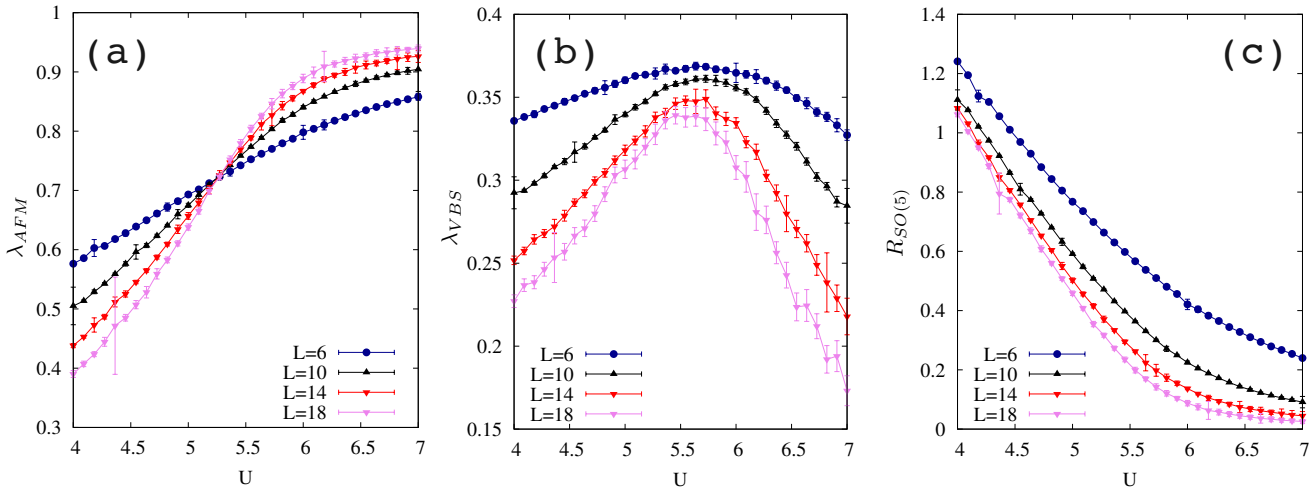

Suppl. Fig. S4: Simulations were carried out at $L = \beta$, $h/t = 0.05$, and $\Delta\tau t = 0.1$. For this choice of h and βt the Ising field are essentially frozen and the flux per plaquette is very close to -1. (a) $\lambda_{\rm AFM}$ as obtained from the susceptibilities. (b) λ_{VBS} as obtained from the susceptibilities. (c) Ratio $R_{SO(5)} = \chi_{\rm VBS}/\chi_{\rm AFM}$.

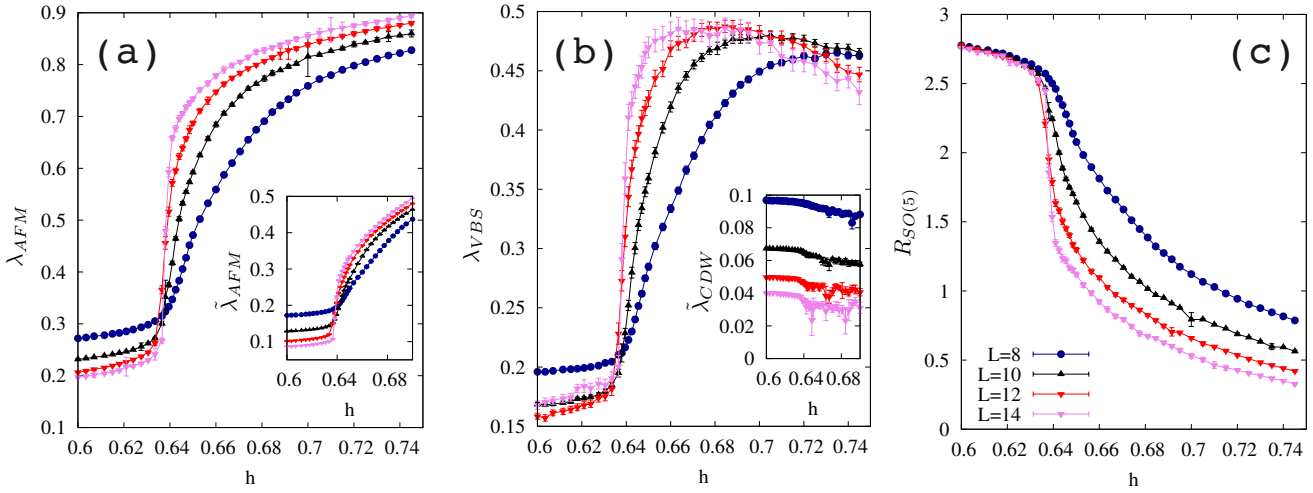

Suppl. Fig. S5: Simulations are carried out at $\beta t = 80$, $U/t = 1$, $\Delta\tau = 0.4$. The temperature was chosen as low as possible so as to attempt to satisfy the constraint. (a) $\lambda_{\rm AFM}$ as obtained from the susceptibilities. Inset: $\tilde{\lambda}_{\rm AFM}$ as obtained from equal time correlation functions. (b) $\lambda_{\rm VBS}$ as obtained from the susceptibilities. Inset: Charge density wave (CDW) correlation ratio at the antiferromgnetic wave vector, $\tilde{\lambda}_{\rm CDW}$, as obtianed from equal time correlation functions. (c) Ratio $R_{SO(5)} = \chi_{\rm VBS}/\chi_{\rm AFM}$.

dominated by the singular part of the free energy and thereby requires $\eta < 2$. Note that the finite size scaling form for susceptibilities reads $\chi \simeq L^{2-\eta} G\left(L^z/\beta, L^{1/\nu}(g-g_c)\right)$. Fig. S4(a) shows $\lambda_{\rm AFM}$ for the O(3)-Gross-Neveu-Yukawa transition [5–7] and clearly pins down the critical value of U/t. The data of Fig. S4(b) is consistent with a constant value of $\lambda_{\rm VBS}$ at the transition and in the thermodynamic limit thereby confirming critical VBS fluctuations at the transition. However, the quotient $\chi_{\rm VBS}/\chi_{\rm AFM}$ clearly shows that at the O(3)-Gross-Neveu-Yukawa transition $\eta_{\rm VBS} > \eta_{\rm AFM}$ since at U_c, the curves fail to cross. Such a statement does not hold for the OSM to AFM transition (see Fig. S5). Here, the data is consistent with $\eta_{\rm VBS} = \eta_{\rm AFM}$ thereby supporting an emergent SO(5) symmetry. The inset of Fig. S5(a) shows the AFM correlation ratio – as obtained form equal time correlation functions. Comparison with the equivalent data for the charge density wave (CDW), inset of Fig. S5(b), shows that the SO(8) symmetry of Dirac fermions is violated at the OSM to AFM transition.

Appendix D: QED$_3$ and confinement transition of $\mathbb{Z}_4$ gauge theory

We consider the following conituum theory

$$\mathcal{L} = \sum_{i=1}^{4} \bar{\psi}_i \not{D}_a \psi_i + \frac{1}{2}|D_{4a}\phi|^2 + r|\phi|^2 + \lambda|\phi|^4 + \frac{1}{4e^2} f_{\mu\nu}^2 + \kappa V + \kappa^* V^*, \tag{D1}$$

where a_μ is a $U(1)$ gauge field, ψ_i is a two-component Dirac fermion with gauge charge $q_g = 1$, ϕ is a complex boson with gauge charge $q_g = 4$, and V schematically represents the monopole (instanton) operator of the $U(1)$ gauge field.

Let us first ignore the monopole term. When $r < r_c$ the Higgs condensate $\langle\phi\rangle \neq 0$ will produce a $\mathbb{Z}_4$ gauge theory with $N_f = 4$ gapless Dirac fermions. When $r > r_c$ the Higgs field can be ignored at low energy, and we get a pure QED$_3$ with $N_f = 4$, which appears to be a stable conformal field theory from numerical studies [8]. The critical point is expected to be also stable since the extra critical Higgs field ϕ should further control the gauge field fluctuation. Therefore in the absence of monopole the above theory describes a continuous transition from $N_f = 4$ $\mathbb{Z}_4$ gauge theory to $N_f = 4$ QED$_3$.

Now put the monopole terms back (assuming such a term is compatible with all global symmetries, as supported by previous study [9]). For the Higgs phase this has no effect. For the QED$_3$ phase, the monopole term is likely relevant [10, 11] ($\Delta_V = 0.265 N_f - 0.038 + O(1/N_f) = 1.022 + O(1/N_f) < 3$), and physically we expect confinement and spontaneous chiral symmetry breaking at low energy, producing a Neel-like state. At the critical point we expect the critical Higgs field to render the monopole irrelevant. This is because even without the gapless Dirac fermions, the monopole is known to be irrelevant because of the critical charge-4 Higgs field [12],

and physically we expect the gapless Dirac fermions to make the monopole even more irrelevant. Therefore at the critical point the $U(1)$ gauge theory is effectively non-compact. Also notice that unlike the QCD_3 scenario for the transition studied in the main text, there is no cubic-like term for the Higgs field. For these reasons we expect the QED_3-Higgs theory to describe a continuous transition is between a $\mathbb{Z}_4$ gauge theory with $N_f = 4$ Dirac fermions and a Neel state.

---

[1] S. Gazit, M. Randeria, and A. Vishwanath, "Emergent Dirac fermions and broken symmetries in confined and deconfined phases of Z_2 gauge theories," Nature Physics **13**, 484 (2017), arXiv:1607.03892 [cond-mat.str-el].

[2] E. Huffman and S. Chandrasekharan, "Fermion bag approach to Hamiltonian lattice field theories in continuous time," Phys. Rev. D **96**, 114502 (2017).

[3] M. Bercx, F. Goth, J. S. Hofmann, and F. F. Assaad, "The ALF (Algorithms for Lattice Fermions) project release 1.0. Documentation for the auxiliary field quantum Monte Carlo code," SciPost Phys. **3**, 013 (2017).

[4] F. F. Assaad and T. Grover, "Simple Fermionic Model of Deconfined Phases and Phase Transitions," Phys. Rev. X **6**, 041049 (2016).

[5] F. Parisen Toldin, M. Hohenadler, F. F. Assaad, and I. F. Herbut, "Fermionic quantum criticality in honeycomb and π-flux Hubbard models: Finite-size scaling of renormalization-group-invariant observables from quantum Monte Carlo," Phys. Rev. B **91**, 165108 (2015).

[6] F. F. Assaad and I. F. Herbut, "Pinning the Order: The Nature of Quantum Criticality in the Hubbard Model on Honeycomb Lattice," Phys. Rev. X **3**, 031010 (2013).

[7] Y. Otsuka, S. Yunoki, and S. Sorella, "Universal Quantum Criticality in the Metal-Insulator Transition of Two-Dimensional Interacting Dirac Electrons," Phys. Rev. X **6**, 011029 (2016).

[8] N. Karthik and R. Narayanan, "Scale invariance of parity-invariant three-dimensional QED," Phys. Rev. D **94**, 065026 (2016), arXiv:1606.04109 [hep-th].

[9] J. Alicea, "Monopole quantum numbers in the staggered flux spin liquid," Phys. Rev. B **78**, 035126 (2008), arXiv:0804.0786 [cond-mat.str-el].

[10] V. Borokhov, A. Kapustin, and X. Wu, "Topological Disorder Operators in Three-Dimensional Conformal Field Theory," Journal of High Energy Physics **11**, 049 (2002), hep-th/0206054.

[11] E. Dyer, M. Mezei, and S. S. Pufu, "Monopole Taxonomy in Three-Dimensional Conformal Field Theories," ArXiv e-prints (2013), arXiv:1309.1160 [hep-th].

[12] J. Manuel Carmona, A. Pelissetto, and E. Vicari, "N-component Ginzburg-Landau Hamiltonian with cubic anisotropy: A six-loop study," Phys. Rev. B **61**, 15136 (2000).